

Electron Spin Echo Envelope Modulation and Extended X-ray Absorption Fine Structure Studies of Active Site Models of Oxygenated Cobalt-Substituted Hemoproteins: Correlating Electron-Nuclear Couplings and Metal–Ligand Bond Lengths

H. Caroline Lee,^{*,§} Eva Scheuring,^{§,†} Jack Peisach,^{§,‡} and Mark R. Chance^{§,†}

Contribution from the Department of Physiology and Biophysics, Center for Synchrotron Biosciences, and Biotechnology Resource in Pulsed EPR Spectroscopy, Albert Einstein College of Medicine of Yeshiva University, Bronx, New York 10461

Received May 27, 1997. Revised Manuscript Received October 1, 1997[⊗]

Abstract: Electron spin echo envelope modulation (ESEEM) and extended X-ray absorption fine structure (EXAFS) spectroscopic studies of oxygenated cobalt (oxyCo) [tetraphenylporphyrin(TPP)][1-methylimidazole (1-MeIm)], an active site model of oxyCo-substituted globins (functional and EPR-active [$S = 1/2$] analogues of oxygen carrying hemoproteins), are carried out in order to examine the correlation of oxygen affinity with electron-nuclear coupling parameters and metal–ligand bond lengths. ESEEM demonstrates that the magnitude of the electron-nuclear hyperfine and nuclear quadrupole couplings to the directly-coordinated ^{14}N of 1-MeIm decrease (A_{iso} , from 3.54 to 3.04 MHz; e^2qQ , from 2.39 to 2.08 MHz) as the solvent composition is varied from 0 to 50% (v/v) dichloromethane in toluene. For oxyCo[(*o*-R)₁TPP][1-MeIm] (where R = –H, –NHCOC(CH₃)₃, –NHCOCH₃, or –NHCONHC₆H₅, an ortho substituent on one of the four meso phenyls of TPP), couplings to the axial nitrogen decrease (A_{iso} , from 3.54 to 3.07 MHz; e^2qQ , from 2.39 to 2.09 MHz) with increased electron-withdrawing strength of R, i.e., with increased acidity of the amide proton of R that may interact with the bound dioxygen. EXAFS measurements, and analysis using *ab initio* EXAFS codes and global mapping, find that the cobalt–axial nitrogen (N_{ax}) bond of oxyCoTPP-1-MeIm shortens by $0.18 \pm 0.06 \text{ \AA}$ when the solvent is changed from 100% toluene ($\text{Co}-N_{\text{ax}} = 2.12 \text{ \AA}$) to 50% toluene/50% dichloromethane ($\text{Co}-N_{\text{ax}} = 1.94 \text{ \AA}$). The average cobalt–equatorial nitrogens (1.94–1.96 \AA) and cobalt–oxygen (1.95–1.98 \AA) distances are unchanged within the error. Similar results were obtained when oxyCoTPP-1-MeIm was compared (in 100% toluene) with its (*o*-NHCONHC₆H₅)₁TPP counterpart, where the cobalt–ligand bond lengths are indistinguishable from those of oxyCoTPP-1-MeIm in 50% toluene/50% dichloromethane. Increasing the polarity of the solvent and of the vicinity of the bound dioxygen increases oxygen affinity of the metal due to an increase in the ionicity of the cobalt–dioxygen bond that is manifested in reduction in electron-nuclear couplings to the axial nitrogen [Lee et al. *Biochemistry* 1994, 33, 7609] and shortening of the cobalt–axial nitrogen bond. These ESEEM and EXAFS characterizations of metal–ligand interactions demonstrate the correlation of electron-nuclear coupling and metal–ligand bond lengths with oxygen affinity of hemoprotein model complexes.

Introduction

Binding of oxygen to the heme iron is central not only to the oxygen transport functions of globins but also to the activation of the wide spectrum of heme enzymes that are involved, for example, in the metabolism of biomolecules, drugs, and xenobiotics (oxygenases, peroxidases), in antimicrobial activities (peroxidases) and in respiration (cytochrome oxidase). Therefore, there have long been intensive efforts, including the use of spectroscopic, kinetic, mutagenesis, and model compound approaches, to elucidate the structural factors that govern oxygen affinity of hemoproteins. However, it has been difficult to simultaneously correlate oxygen affinity with both the molecular and electronic structures of the oxygenated ferrous (oxyFe)¹ forms of these proteins because of the limited number of crystal

structures available, the fast autooxidation rates of these proteins, and the fact that they are EPR-silent. This problem can partly be resolved by one well-developed technique that involves replacing the heme with cobalt protoporphyrin IX² to generate an oxygenated hemoprotein that has a slower autooxidation rate and a metal center ($S = 1/2$) amenable for EPR studies.

Previous ESEEM studies of oxygenated cobalt(II) protoporphyrin IX-substituted (oxyCo) globins have shown that electron-nuclear hyperfine and nuclear quadrupole coupling to the cobalt-bound $^{14}\text{N}_e$ of the proximal (axial) histidyl imidazole are related to the ionicity of the trans cobalt–dioxygen bond.^{3–5} This interpretation is derived from a molecular orbital model for the Co–O–O unit⁶ that contains a fully occupied σ -bonding orbital, $\text{sp}^2(\text{N}_e) + \text{d}_z^2(\text{Co}) + \pi^*(\text{O}_2)$, and a half-occupied anti-bonding orbital, $\pi^*(\text{O}_2)$. This model predicts that electron-nuclear hyperfine coupling to the axial nitrogen, which occurs through

(2) Hoffman, B. M.; Petering, D. H. *Proc. Natl. Acad. Sci. U.S.A.* 1970, 67, 637.

(3) Lee, H. C.; Ikeda-Saito, M.; Yonetani, T.; Magliozzo, R. S.; Peisach, J. *Biochemistry* 1992, 31, 7274.

(4) Lee, H. C.; Wittenberg, J. B.; Peisach, J. *Biochemistry* 1993, 32, 11500.

(5) Lee, H. C.; Peisach, J.; Dou, Y.; Ikeda-Saito, M. *Biochemistry* 1994, 33, 7609.

(6) Tovrog, B. S.; Kitko, D. J.; Drago, R. S. *J. Am. Chem. Soc.* 1976, 98, 5144.

* Author to whom correspondence should be addressed.

§ Department of Physiology and Biophysics.

† Center for Synchrotron Biosciences.

‡ Biotechnology Resource in Pulsed EPR Spectroscopy.

⊗ Abstract published in *Advance ACS Abstracts*, November 15, 1997.

(1) Abbreviations: EPR, electron paramagnetic resonance; ESEEM, electron spin echo envelope modulation; EXAFS, extended X-ray absorption fine structure; 1-MeIm, 1-methylimidazole; oxyCo hemoproteins; oxygenated hemoproteins of which the heme has been substituted by a Co(II)-protoporphyrin IX; PF, "picket fence" porphyrin, [*meso*-tetrakis($\alpha,\alpha,\alpha,\alpha$ -*o*-pivalamidophenyl)porphyrin]; TPP, tetraphenylporphyrin.

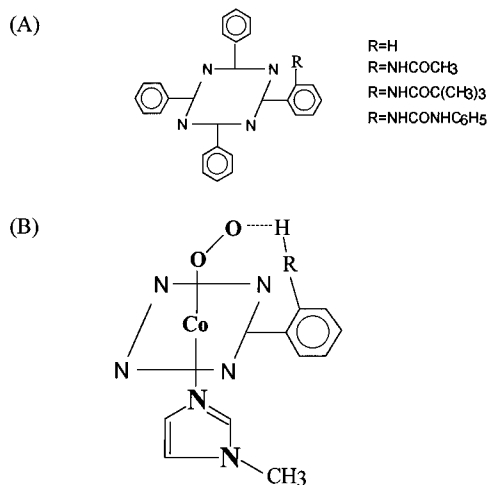


Figure 1. (A) Structures of monosubstituted tetraphenylporphyrin derivatives where an electron-withdrawing group R replaces the ortho proton on one of the meso phenyls which orients perpendicularly to the porphyrin plane. (B) Proposed interaction between the amide proton on R and the bound dioxygen.

spin polarization of the fully occupied σ -bonding orbital,⁷ decreases with a decrease in the cobalt character, or increase in the oxygen character, of this orbital. Similarly, ^{14}N nuclear quadrupole coupling, which decreases with an increase in axial nitrogen sp^2 lone-pair electron donation to cobalt,^{8,9} also decreases with a decrease in the cobalt character of the σ -bonding orbital. In this way, reductions in ^{14}N electron-nuclear couplings observed for oxyCo globins are directly correlated with an increase in ionicity of the cobalt–dioxygen bond,⁵ i.e., its electronic configuration more likely resembles $\text{Co}^{3+}-\text{O}_2^{\cdot-}$ than $\text{Co}^{2+}-\text{O}_2$. Consequently, a shorter cobalt–dioxygen bond is predicted.¹⁰ Furthermore, increased lone-pair electron donation to cobalt, induced by an increase in the ionicity of the cobalt–dioxygen bond and manifested as reduction in nuclear quadrupole coupling, indicates an increased overlap of the nitrogen sp^2 orbital and the d_z^2 orbital of cobalt, thus a shorter cobalt–axial nitrogen bond is also predicted.¹⁰ Increase in the ionicity of the cobalt–dioxygen bond, or increased oxygen character in the σ -bonding orbital, should also lead to an increase in oxygen affinity.^{3,5}

The correlation of ionicity of metal–oxygen bond with ^{14}N electron-nuclear couplings, metal–ligand bond length, and oxygen affinity is examined in this study. One goal is to estimate the magnitude and distribution of bond length changes, implied by changes in electronic structures, throughout the metal–ligand system. ESEEM and EXAFS spectroscopy are applied to a model compound of oxyCo globins, oxyCoTPP-1-MeIm, whereby the ionicity of cobalt–dioxygen bond is systematically altered in two ways. First, solvent systems with increasing polarity are used. Second, the ortho proton on one of the four meso phenyls of TPP is replaced by substituents R (where R is $-\text{NHCOCH}_3$, $-\text{NHCOC}(\text{CH}_3)_3$, or $-\text{NHCONHC}_6\text{H}_5$), with different electron-withdrawing strength (Figure 1A). The acidic proton on R can interact with the cobalt-bound dioxygen as shown in Figure 1B (see Discussion). An increase in the electron-withdrawing strength of R increases the acidity

of the amide proton and thus the ionicity of the cobalt–dioxygen bond. (The choice of 1-MeIm as axial ligand precludes interactions at the noncoordinating nitrogen that may complicate interpretation of results.) Increase in the polarity of the solvent and of the vicinity of the bound dioxygen have been shown to increase oxygen affinity of both cobalt and iron porphyrin model systems (see Discussion).

This study finds that for systems exhibiting higher oxygen affinity as a result of increased polarity of the solvent or the polarity of the dioxygen environment, reductions in ^{14}N electron-nuclear couplings occur that are also accompanied by shortening of the cobalt–axial nitrogen bonds, whereas the cobalt–oxygen bond length remains comparatively unaffected. This study reveals a correlation between electronic structure of cobalt–dioxygen bond of hemoprotein model complexes and cobalt–axial nitrogen bond length change as well as electron-nuclear coupling parameters. The sensitive communication between the two axial metal–ligand bonds in governing oxygen affinity is illustrated.

Materials and Methods

Sample Preparation. Co(II)TPP, specialty chemicals (pyrrole, benzaldehyde, *o*-nitrobenzaldehyde, tin chloride, acetyl chloride, pivaloyl chloride, phenyl isocyanate, 1-methylimidazole), and solvents (propionic acid, pyridine, benzene, methanol, toluene, dichloromethane) were obtained from Aldrich Chemical Company. Substituted TPPH₂ were prepared by first synthesizing a mixture of TPP and nitrophenylporphyrins using a modified procedure^{11,12} of the Alder synthesis.¹³ The (*o*-nitro)₁TPPH₂ isomer was isolated by gravity chromatography on silica gel (Baker chromatographic grade) in toluene. The nitro group was then reduced to amino by the SnCl_2/HCl method.¹⁴ (*o*-NH₂)₁-TPPH₂, purified on a silica gel column in toluene, was used to synthesize (*o*-NHCOCH₃)₁TPPH₂,¹⁵ (*o*-NHCOC(CH₃)₃)₁TPPH₂,¹⁵ and (*o*-HNCONHC₆H₅)₁TPPH₂¹⁶ according to published methods. Insertion of cobalt followed a published procedure^{11,12} using a 3:1 (v/v) mixture of dichloromethane and methanol. The CoTPP derivatives were purified on a silica gel column in toluene before use.

ESEEM and EXAFS samples contained 2–5 mM of CoTPP or its derivatives and 0.1% (v/v) 1-methylimidazole^{17,18} in toluene or a mixture of toluene/dichloromethane (see Results). Toluene and dichloromethane were distilled, dried over 8–12 mesh molecular sieve overnight, and purged with oxygen immediately before using. ESEEM samples were prepared by addition of solvent, followed by 1-methylimidazole, to CoTPP or a derivative. The mixture was frozen in liquid nitrogen under atmospheric pressure. EPR spectroscopy was used to ensure complete oxygenation^{15,17,19,20} of the samples before ESEEM studies. EXAFS samples were prepared by transferring ESEEM samples, in air, to lucite sample holder, and freezing in liquid nitrogen. EPR spectroscopy showed that $\leq 10\%$ oxidation and/or deoxygenation occurred during the time course required for preparing a EXAFS sample from a fully oxygenated ESEEM sample.

EPR and ESEEM Spectroscopy. Continuous wave EPR spectra were recorded at 77 K on a Varian E112 spectrometer, equipped with a Systron-Donner frequency counter. ESEEM data were recorded at 4.2 K on a pulsed EPR spectrometer²¹ using a folded stripline cavity²²

(11) Walker, F. A.; Balke, V. L.; McDermott, G. A. *J. Am. Chem. Soc.* **1982**, *104*, 1569.

(12) Walker, F. A.; Balke, V. L.; McDermott, G. A. *Inorg. Chem.* **1982**, *21*, 3342.

(13) Alder, A. D.; Longo, F. R.; Finarelli, J. D.; Goldmacher, J.; Assour, J.; Korsakoff, L. *J. Org. Chem.* **1967**, *32*, 476.

(14) Collman, J. P.; Gagne, R. R.; Reed, C. A.; Halbert, T. R.; Lang, G.; Robinson, W. T. *J. Am. Chem. Soc.* **1975**, *97*, 1427.

(15) Walker, F. A.; Bowen, J. *J. Am. Chem. Soc.* **1985**, *107*, 7632.

(16) Wuenschell, G. E.; Tetreau, C.; Lavalette, D.; Reed, C. A. *J. Am. Chem. Soc.* **1992**, *114*, 3346.

(17) Walker, F. A. *J. Am. Chem. Soc.* **1970**, *92*, 4235.

(18) Walker, F. A. *J. Am. Chem. Soc.* **1973**, *95*, 1150.

(19) Hoffman, B. M.; Diemente, D. L.; Basolo, F. *J. Am. Chem. Soc.* **1970**, *92*, 61.

(20) Walker, F. A. *J. Magn. Reson.* **1974**, *15*, 201.

(7) Wayland, B. B.; Abd-Elmageed, M. E. *J. Am. Chem. Soc.* **1974**, *98*, 4809.

(8) Hsieh, Y.-N.; Rubenacker, G. V.; Cheng, C. P.; Brown, T. L. *J. Am. Chem. Soc.* **1977**, *99*, 1384.

(9) Ashby, C. I. H.; Cheng, C. P.; Brown, T. L. *J. Am. Chem. Soc.* **1978**, *100*, 6057.

(10) Lee, H. C.; Peisach, J.; Tsuneshige, A.; Yonetani, T. *Biochemistry* **1995**, *34*, 6883.

that can accommodate standard 4 mm, o.d., EPR tubes. Three-pulse, or stimulated echo, experiments²³ were conducted at 8.6 GHz as described previously.⁵

ESEEM spectra were simulated using angle-selection methods²⁴ and followed a published procedure.⁵ The ¹⁴N spin Hamiltonian is given in eq 4 (see Results). The nuclear hyperfine tensor is taken to be axial, described by an isotropic nuclear hyperfine coupling constant, A_{iso} , and an anisotropic coupling constant, $F = g_N \beta_N g_e \beta_e / (r_{\text{eff}})^3$, where r_{eff} is the effective dipole distance. Two angles, θ_N and ϕ_N , relate the orientation of the hyperfine tensor with the \mathbf{g} tensor. The nuclear quadrupole tensor is described by a nuclear quadrupole coupling constant, e^2qQ , and an asymmetry parameter, η , that are related to the principal values (q_{xx} , q_{yy} , q_{zz}) of the electric field gradient tensor by

$$e^2qQ = e^2q_{zz}Q \quad (1)$$

$$\eta = (q_{yy} - q_{xx})/q_{zz} \quad (2)$$

where $|q_{zz}| > |q_{yy}| > |q_{xx}|$. Three Euler angles α , β , and γ relate the orientation of the nuclear quadrupole tensor to that of the \mathbf{g} tensor. All simulations were carried out on a Microvax II or a Silicon Graphics Indigo computer.

EXAFS Spectroscopy. EXAFS data were collected at the National Synchrotron Light Source (NSLS), Brookhaven National Laboratory (Upton, NY), on beamline X-9B using a sagittally focused Si[111] crystal monochromator. A Ni mirror at an angle of 4.5 milliradians was used to reject higher-order harmonic contamination. Approximately 4 mrad of bending magnet radiation was focused with a horizontal aperture of 2 mm and a vertical slit set at 1 mm. The monochromated photon flux was 2×10^{11} photons s^{-1} at 100 mA beam current. Data were taken in the range of 150–250 mA. Experiments were carried out at 150 K in a closed cycle helium cryostat and at atmospheric pressure to minimize evaporation or sublimation of solvent. EXAFS data were collected with a 0.05 \AA^{-1} step size in k space starting at a photoelectron energy of 1 \AA^{-1} . Below 1 \AA^{-1} , data were collected by counting at a specific energy for 2 s and incrementing the energy by 10 eV from 100 eV below the cobalt edge to 20 eV below the edge and then in 2.0 eV steps up to 1 \AA^{-1} . Cobalt K- α fluorescence was detected using a 13-element germanium detector.²⁵ Data collection, detector, count rates, energy calibrations, and other techniques have been described previously for cobalt EXAFS.^{26–28} Data were collected for two samples of oxyCoTPP-1-MeIm in 100% toluene and one sample each for oxyCoTPP-1-MeIm in 50% toluene/50% dichloromethane and for oxyCo[*o*-NHCONHC₆H₅]₁TPP-1-MeIm in 100% toluene.

The experimental data were processed with a PC-based version of the AT&T Bell Labs EXAFS package.²⁶ Sharp glitches, caused by nonstatistical events, were removed before further data processing by fitting a polynomial in the appropriate region. Data manipulation with the use of a linear pre-edge fit, cubic polynomial spline background (isolated atom) subtraction, wavevector cubed weighting, Fourier transformation, filter, and back-transform have all been described previously.^{29,30}

EXAFS data were analyzed in an automated procedure using the program AUTOFIT (v. 1.0) as described earlier.³¹ AUTOFIT utilizes

(21) McCracken, J.; Peisach, J.; Dooley, D. M. *J. Am. Chem. Soc.* **1987**, *109*, 4064.

(22) Britt, R. D.; Klein, M. P. *J. Magn. Reson.* **1987**, *75*, 535.

(23) Peisach, J.; Mims, W. B.; Davis, J. L. *J. Biol. Chem.* **1979**, *254*, 12379.

(24) Cornelius, J. B.; McCracken, J.; Clarkson, R. B.; Belford, R. L.; Peisach, J. *J. Phys. Chem.* **1990**, *94*, 6977.

(25) Cramer, S. P.; Chen, J.; George, S. J.; van Elp, J.; Moore, J.; Tensch, O.; Colaresi, J.; Yocum, M.; Mullins, O. C.; Chen, C. T. *Nucl. Instrum. Methods A* **1992**, *319*, 1, 285.

(26) Scheuring, E. M.; Sagi, I.; Chance, M. R. *Biochemistry* **1994**, *33*, 6310.

(27) Wirt, M. D.; Kumar, M.; Ragsdale, S. W.; Chance, M. R. *J. Am. Chem. Soc.* **1993**, *115*, 2146.

(28) Wirt, M. D.; Kumar, M.; Wu, J.-J.; Scheuring, E. M.; Ragsdale, S. W.; Chance, M. R. *Biochemistry* **1995**, *34*, 5269.

(29) Chance, M. R.; Powers, L.; Kumar, C.; Chance, B. *Biochemistry* **1986**, *25*, 1259.

(30) Chance, M. R.; Powers, L.; Poulos, L.; Chance, B. *Biochemistry* **1986**, *25*, 1266.

the *ab initio* X-ray absorption code FEFF (v. 6.01)^{32,33} to calculate the theoretical amplitude and phase functions. The starting structure for the calculations is generated by selecting an appropriate structure from the Cambridge Crystallographic database³⁴ and then using the molecular modeling package Chem-X (Chemical Design Ltd., England) to manipulate the starting structure. The starting structure, in this case oxyFe[PF][1-MeIm],³⁵ is then altered by AUTOFIT to generate an input file for the FEFF calculations. For the structure above, one bond of each methene bridge is clipped so that the pyrroles can be moved as independent units. The iron atom was replaced with cobalt, all atoms further than 5 \AA from cobalt were deleted, and the bond angles were left unchanged relative to the database values. For example, the Co–O–O bond angle used was 131°, the Fe–O–O angle of oxyFe[PF][1-MeIm], from which the starting structure for FEFF calculation was derived.³⁵ The crystal structure of the model compound has two of the pyrrole nitrogen average distances at 1.96 \AA and two at 0.02 \AA longer; this difference was maintained in the simulations. However, only the average of all four distances is reported.

In the FEFF input file only a few parameters are set, such as the amplitude reduction factor (S_o^2 , 0.85) and the number of scattering paths (NLEG = 5). In this study, the Debye-Waller parameters were adjusted in the fitting program. The simulated k^3 weighted $\chi(k)$ data are Fourier filtered with a wide window (0.4–4.8 \AA) and back-transformed to produce the amplitude and phase functions. This simulation is then compared to unfiltered EXAFS experimental data with identical k -range (typically 4–12 \AA^{-1}) by a one-atom fitting procedure fixing the distance (r) and the coordination number (N) and letting the threshold energy (E_o), and the Debye-Waller factor ($\Delta\sigma^2$), to float. For all the solutions reported, these values were maintained in a reasonable chemical range.³¹ The goodness of fit is given in the form of the residual sum squared

$$\sum R^2 = \sum_i \{ (k^3 \chi_i)_{\text{experimental}} - (k^3 \chi_i)_{\text{simulation}} \}^2 \quad (3)$$

The error analysis is based on methods described earlier^{31,36,37} and uses Fourier filtered EXAFS data with the same filter window and k -range as the simulated data. The distances obtained by analyzing unfiltered data are identical to those in which both experimental and simulated data are filtered and back-transformed.

For each analysis, numerous structures are generated by varying selected distance parameters, after the FEFF calculations each simulated EXAFS spectrum is compared to the experimental $k^3\chi(k)$ data, and all fitting results are recorded in a single file. The final results are presented as pseudo-3D contour plots in which the $\sum R^2$ values are represented as shaded contours, with the darker areas indicating a better fit, while the two distance parameters that are varied are plotted as the x - and y -axes. The three distances of interest are those from cobalt to the two axial ligands and the average distance from cobalt to the porphyrin nitrogens.

Results

EPR and ESEEM Spectroscopy. The 1-MeIm complex of oxyCoTPP and its (*o*-R)₁TPP counterparts exhibit EPR spectra typical for complexes of oxyCo[porphyrin] with nitrogenous axial ligand.^{17,19,20} These spectra, exemplified by that of oxyCoTPP-1-MeIm in toluene (Figure 2), arise from an unpaired electron in a π^* orbital of the bound O₂,^{6,19,38,39} center around $g = 2$ and show splittings due to hyperfine interaction with the

(31) Chance, M. R.; Miller, L. M.; Fischetti, R. F.; Scheuring, E.; Huang, W.-X.; Sclavi, B.; Hai, Y.; Sullivan, M. *Biochemistry* **1996**, *35*, 9014–9023.

(32) Rehr, J. J.; Leon, J. M. D.; Zabinsky, S. I.; Albers, R. C. *J. Am. Chem. Soc.* **1991**, *113*, 5135.

(33) Rehr, J. J.; Albers, R. C.; Zabinsky, S. I. *Phys. Rev. Lett.* **1992**, *69*, 3397.

(34) Allen, F. H.; Kennard, O.; Taylor, R. *Acc. Chem. Res.* **1983**, *16*, 146.

(35) Jameson, G. B.; Rodley, G. A.; Robinson, W. T.; Gagne, R. R.; Reed, C. A.; Collman, J. P. *Inorg. Chem.* **1978**, *17*, 850.

(36) Lytle, F. W.; Sayers, D. E.; Stern, E. A. *Phys. B* **1989**, *158*, 701.

(37) Powers, L.; Kincaid, B. M. *Biochemistry* **1989**, *28*, 4461.

(38) Getz, D.; Melamud, E.; Silver, B. L.; Dori, Z. *J. Am. Chem. Soc.* **1975**, *97*, 3846.

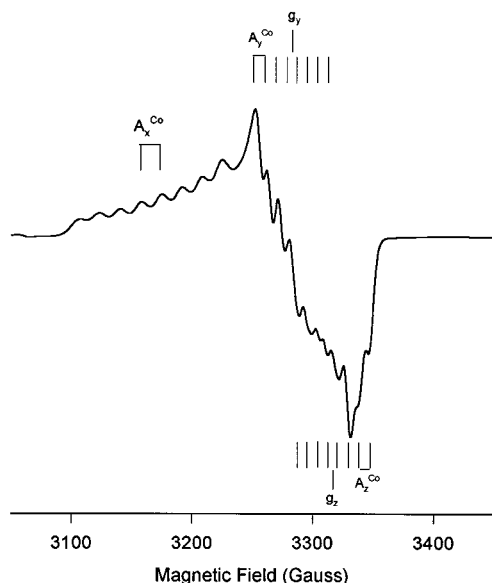


Figure 2. EPR spectra of oxyCoTPP-1-MeIm in 100% toluene. Spectra were collected at microwave frequency = 9.12 GHz, microwave power = 5 mW, modulation amplitude = 5 G, and temperature = 77K.

^{59}Co nucleus. Single crystal EPR studies^{40–43} of oxyCo Mb have shown that the g and cobalt hyperfine tensors for these systems are coincident and are rhombic ($g_x > g_y > g_z$), with small differences between g_y and g_z as well as between A_y^{Co} and A_z^{Co} . In frozen solution, g_x and A_x^{Co} can be easily obtained from the EPR spectrum since all eight cobalt hyperfine lines are resolved in the perpendicular region of the spectrum (Figure 2). A_y^{Co} and A_z^{Co} can be estimated from the splittings in the middle and in the end of the spectrum, respectively. These values are used to locate the magnetic field half way between the fourth ($m_l^{\text{Co}} = 1/2$) and fifth ($m_l^{\text{Co}} = -1/2$) cobalt hyperfine lines, assuming the absence of any other mechanisms that may broaden individual m_l^{Co} lines. g_y and g_z are then calculated from these magnetic field settings as shown in Figure 2. The g values and cobalt hyperfine coupling constants for the complexes studied are summarized in Table 1.

Interactions between the unpaired electron and the directly-coordinate ^{14}N of 1-MeIm give rise to ESEEM spectra shown in Figures 3 and 4.^{3,44} The coupled ^{14}N is described by the spin Hamiltonian:

$$\hat{H}_N = -g_N \beta_N \mathbf{B} \cdot \mathbf{I} + S \mathbf{A}_N \cdot \mathbf{I} + (e^2 q Q / 4) [3I_z^2 - 2 + \eta(I_x^2 - I_y^2)] \quad (4)$$

Here \mathbf{B} is the magnetic field, S and \mathbf{I} are the electronic and nuclear spin operators and β_N is the nuclear magneton. The first, second, and third term in eq 4 describes the nuclear Zeeman, electron-nuclear hyperfine, and nuclear quadrupole interaction, respectively.

The spectra shown in Figures 3 and 4 are characteristic for a coupled ^{14}N nucleus⁴⁵ at conditions of near “exact cancella-

tion”,⁴⁶ i.e., the magnitude of the nuclear Zeeman interaction is about half of that of the nuclear hyperfine coupling. The low-frequency lines (those < 3 MHz in Figures 3 and 4) arise from the electron-spin manifold where the nuclear Zeeman interaction essentially cancels that for the nuclear hyperfine interaction (eq 4). The frequency of the two $\Delta m_l = 1$ (ν_0, ν_-) and one $\Delta m_l = 2$ (ν_+) transitions in this electron-spin manifold are related to the nuclear quadrupole coupling constant, $e^2 q Q$, and the asymmetry factor, η , by

$$\nu_{\pm} = \frac{3}{4} e^2 q Q (1 \pm \eta/3) \quad (5)$$

$$\nu_0 = \frac{1}{2} e^2 q Q \eta \quad (6)$$

The highest frequency line in the ESEEM spectra arises from the $\Delta m_l = 2$ transition in the other electron spin manifold where the nuclear Zeeman interaction adds to the nuclear hyperfine interaction.⁴⁵

Figure 3 shows that the ESEEM spectrum of oxyCoTPP-1-MeIm is altered as increasing percentage (v/v) of dichloromethane in toluene is used. The two highest frequency spectral components shift to lower frequencies as a result of increasing polarity of the solvent, indicating a reduction in axial ^{14}N electron-nuclear couplings. When one of the phenyl orthoprotons of oxyCoTPP-1-MeIm is substituted by an electron-withdrawing group, R (where R is $-\text{NHCOC}(\text{CH}_3)_3$, $-\text{NHCOCH}_3$, and $-\text{NHCONHC}_6\text{H}_5$), the two highest frequency ESEEM spectral components again shift to lower frequencies as the electron-withdrawing strength of R increases (Figure 4). The studies shown in Figures 3 and 4 aim at examining changes in the ESEEM spectrum of oxyCoTPP-1-MeIm resulting from changes in the electronic structure of the cobalt–dioxygen bond (see Discussion). For this reason, 1-MeIm is chosen as the axial ligand to eliminate any effects at the nonbonded remote nitrogen that may complicate the interpretation of ESEEM results.

Spectra shown in Figures 3 and 4 are analyzed by simulation using angle-selection methods.²⁴ The simulations involved varying individual parameters manually and determining the fit by inspection. The g tensor used in the simulations follows the assignment of Hori et al.^{42,43} which places g_z (g_{min}) along the O–O bond and g_x (g_{max}) along the unpaired electron-containing π^* orbital. The ^{14}N hyperfine tensor and the nuclear quadrupole tensor are taken to be coincident,⁵ with both the electron- ^{14}N nuclear vector⁷ and q_{zz} ^{8,9} along the Co–axial nitrogen bond. For this reason, the angles between electron- ^{14}N nuclear vector and g_z , θ_N , and the angle between q_{zz} and g_z , β , are assumed to be equal.

In a typical simulation, the coupling parameters A_{iso} , $e^2 q Q$, and η (see Materials and Methods) are first varied to obtain a frequency match for data collected at $g = 2.03$. Spectra collected at two other g values (1.99, 2.08) are then simulated (with adjustment of the coupling parameters obtained for the $g = 2.03$ setting) to determine values for the angle β ($=\theta_N$). Appropriate values for these angles are those that require the least adjustment of the coupling parameters (A_{iso} , $e^2 q Q$, and η) to fit data at different g values. The range of parameters used in fitting spectra at the three g values defines the uncertainties in the simulations. The uncertainties of the angles are the range that produces a $\leq 10\%$ change in the intensity of one or more spectral components at a single magnetic field. The effect of varying r_{eff} , ϕ_N , α , and γ on the simulations are then evaluated independently using previously determined values for A_{iso} , $e^2 q Q$, η , β , and θ_N (see footnotes a and b, Table 2).

(39) Dedieu, A.; Rohmer, M.-M.; Veillard, A. *J. Am. Chem. Soc.* **1976**, *98*, 5789.

(40) Chien, J. W. C.; Dickinson, L. C. *Proc. Natl. Acad. Sci. U.S.A.* **1972**, *69*, 2783.

(41) Dickinson, L. C.; Chien, J. C. W. *Proc. Natl. Acad. Sci. U.S.A.* **1980**, *77*, 1235.

(42) Hori, H.; Ikeda-Saito, M.; Yonetani, T. *Nature* **1980**, *288*, 501.

(43) Hori, H.; Ikeda-Saito, M.; Yonetani, T. *J. Biol. Chem.* **1982**, *257*, 3636.

(44) Magliozzo, R. S.; McCracken, J.; Peisach, J. *Biochemistry* **1987**, *26*, 7923.

(45) Mims, W. B.; Peisach, J. *J. Chem. Phys.* **1978**, *69*, 4921.

(46) Flanagan, H. L.; Singel, D. J. *J. Chem. Phys.* **1987**, *87*, 5606.

Table 1. EPR Parameters of Oxy (*o*-R)₁TPP-Co-1-MeIm Complexes^a

R	g_x	g_y	g_z	A_x^{Co} (MHz)	A_y^{Co} (MHz)	A_z^{Co} (MHz)	$\rho_{3d}(\text{Co})^b$
H (in 100% toluene)	2.084	2.010	1.989	51.04	28.13	19.13	0.0914
H (in 90% toluene, 10% CH ₂ Cl ₂)	2.079	2.006	1.985	50.91	28.07	20.83	0.0885
H (in 50% toluene, 50% CH ₂ Cl ₂)	2.083	2.007	1.985	47.37	28.09	20.83	0.0832
NHCOC(CH ₃) ₃ ^c	2.080	2.004	1.984	50.93	28.04	20.82	0.0885
NHCOCH ₃ ^c	2.082	2.003	1.987	51.31	28.21	24.49	0.0837
NHCONHC ₆ H ₅ ^c	2.082	2.012	1.989	50.99	21.12	20.88	0.0780

^a Estimated from frozen solution spectra (see Results and Figure 2). ^b The 3d orbital spin density of cobalt, given by the ratio of the observed anisotropy of the cobalt hyperfine to the anisotropy for one full electron in a 3d orbital,⁷ 438 MHz.⁷⁵ The observed anisotropy is given by $A_z - \langle A \rangle$, where $\langle A \rangle$ equals $\frac{1}{3}A_z + \frac{2}{3}(A_x + A_y)$. ^c In 100% toluene.

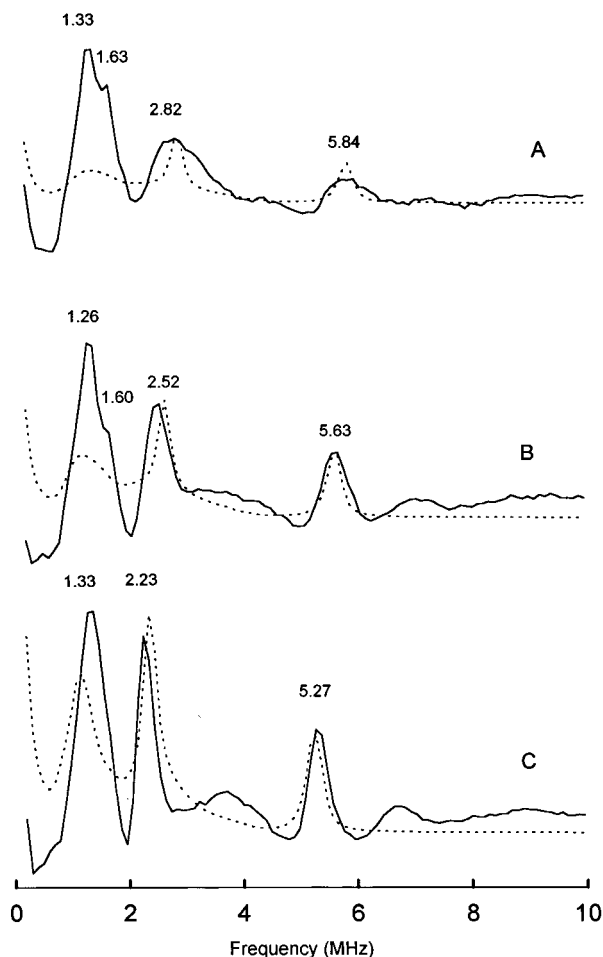


Figure 3. ESEEM spectra of oxyCoTPP-1-MeIm in (A) 100% toluene, (B) 90% toluene, 10% dichloromethane, and (C) 50% toluene, 50% dichloromethane. Experimental conditions were (A) microwave frequency = 8.62 GHz, magnetic field = 3034 G, τ = 155 ns, temperature = 4.2 K; (B) microwave frequency = 8.68 GHz, magnetic field = 3053 G, τ = 154 ns, temperature = 4.2 K; (C) microwave frequency = 8.60 GHz, magnetic field = 3027 G, τ = 155 ns, temperature = 4.2 K. Solid lines, data; dotted lines, best fit simulations using parameters given in Table 2. The numbers indicate peak positions in the data.

The best fit simulations (dotted lines) are compared to data in Figures 3 and 4, and simulation parameters are summarized in Table 2. Reduction in both nuclear hyperfine and nuclear quadrupole couplings occurs with increased solvent polarity or with increased electron withdrawing strength of the ortho substituent, R, on one of the phenyl group of TPP.

EXAFS Spectroscopy. The EXAFS data for the oxyCoTPP-1-MeIm complex in 100% toluene compared to data for the complex in 50% toluene/50% dichloromethane (v/v) are shown in Figure 5A. There is significant increase in amplitude and decrease in frequency of the EXAFS oscillations induced when the solvent polarity is increased. The EXAFS data suggest a

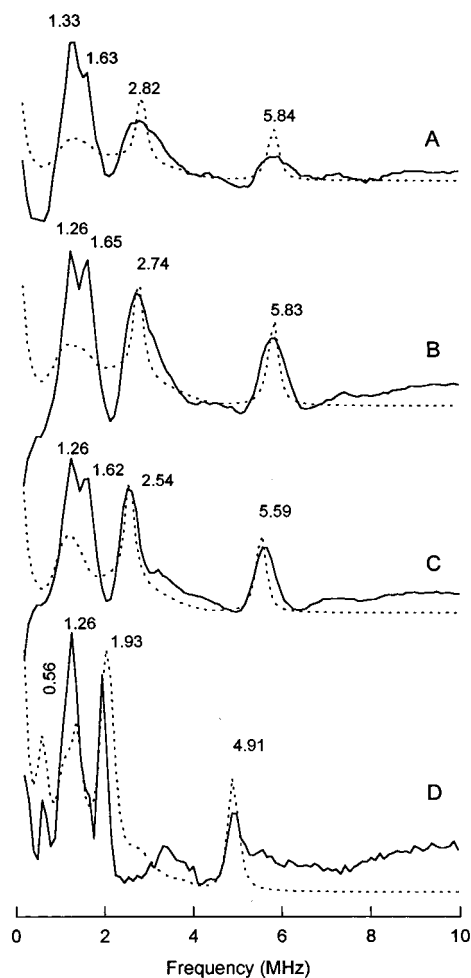


Figure 4. ESEEM spectra of oxyCo(*o*-R)₁TPP-1-MeIm in toluene, where R = (A) -H, (B) -NHCOC(CH₃)₃, (C) -NHCOCH₃ and (D) -NHCONHC₆H₅. Experimental conditions were (A) microwave frequency = 8.62 GHz, magnetic field = 3034 G, τ = 155 ns, temperature = 4.2 K; (B) microwave frequency = 8.59 GHz, magnetic field = 3024 G, τ = 155 ns, temperature = 4.2 K; (C) microwave frequency = 8.60 GHz, magnetic field = 3026 G, τ = 155 ns, temperature = 4.2 K; (D) microwave frequency = 8.69 GHz, magnetic field = 3060 G, τ = 154 ns, temperature = 4.2 K. Solid lines, data; dotted lines, best fit simulations using parameters given in Table 2. The numbers indicate peak positions in the data.

significant shortening of some or all bond lengths in the presence of 50% dichloromethane. A comparison of the oxyCoTPP-1-MeIm complex in 50% toluene/50% dichloromethane to oxyCo-[(*o*-NHCONHC₆H₅)₁TPP][1-MeIm] in 100% toluene is shown in Figure 5B. The spectra of these complexes appear nearly identical, suggesting similar metal-ligand bond lengths.

In order to deconvolute the individual bond lengths from the sum of frequencies reflected in the EXAFS data, simulations of EXAFS spectra were carried out using the *ab initio* EXAFS code FEFF 6.01. The starting structure for the FEFF simulations

Table 2. Electron-Nuclear Coupling Parameters for the Axial Nitrogen in Oxy (*o*-R)₁TPP-Co-1-MeIm Complexes^a

R	A _{iso} (MHz)	r _{eff} ^b (Å)	e ² qQ (MHz)	η	θ _N = β ^c
H (in 100% toluene)	3.54 ± 0.06	3.4 ± 0.2	2.39 ± 0.07	0.88 ± 0.13	13 ± 16°
H (in 90% toluene, 10% CH ₂ Cl ₂)	3.34 ± 0.10	3.4 ± 0.2	2.25 ± 0.05	0.86 ± 0.15	8 ± 5°
H (in 50% toluene, 50% CH ₂ Cl ₂)	3.04 ± 0.06	3.4 ± 0.2	2.08 ± 0.04	0.91 ± 0.08	23 ± 9°
NHCOC(CH ₃) ₃ ^c	3.59 ± 0.05	3.6 ± 0.2	2.24 ± 0.02	0.90 ± 0.04	10 ± 9°
NHCOCH ₃ ^c	3.29 ± 0.05	3.6 ± 0.2	2.21 ± 0.02	0.86 ± 0.06	13 ± 6°
NHCONHC ₆ H ₅ ^c	3.07 ± 0.05	3.6 ± 0.2	2.09 ± 0.05	0.49 ± 0.05	43 ± 3°

^a Obtained from simulation of ESEEM spectra. All simulations utilized φ_N = 0°, α = 0°, and γ = 0°. Varying the angles φ_N, α, and γ has little effect on the simulations. ^b The highest frequency spectral component, the Δm_l = 2 line, of the complexes studied shifts minimally in ESEEM spectra collected at three magnetic field (g = 2.08, 2.03, 1.99) across the EPR absorption, indicating a highly isotropic ¹⁴N hyperfine tensor. The effective dipole distances, r_{eff}, reported here are the lowest values for this parameter that generate isotropic ESEEM simulations. Using r_{eff} smaller than those reported in simulations produces magnetic field-dependent shifts in the Δm_l = 2 line that are larger than those observed in the data. ^c See text. In 100% toluene.

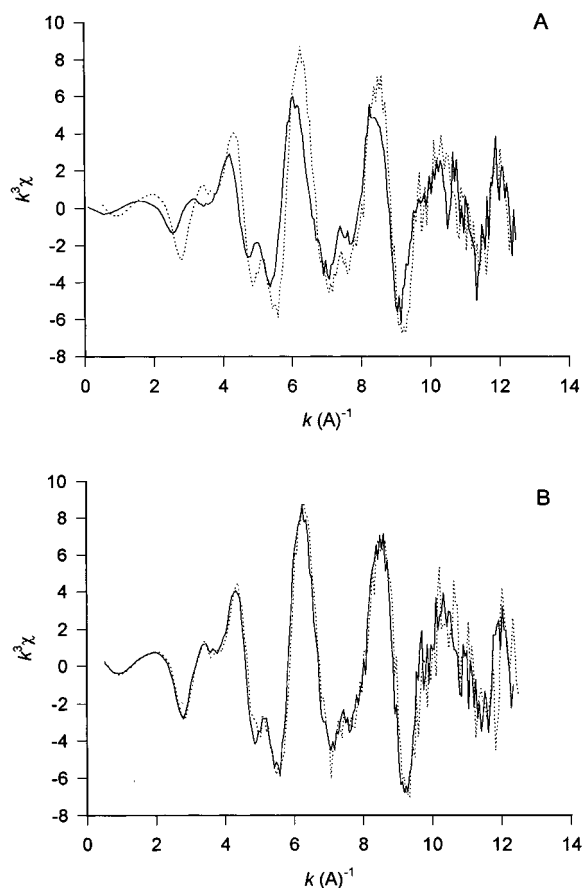


Figure 5. (A) EXAFS spectra of oxyCoTPP-1-MeIm in 100% toluene (solid line) and the same complex in 50% toluene/50% dichloromethane (dashed line). (B) EXAFS spectra of oxyCoTPP-1-MeIm in 50% toluene/50% dichloromethane (solid line) and oxyCo(*o*-NHCONHC₆H₅)₁-TPP-1-MeIm in 100% toluene (dotted line).

was derived from the crystal structure of oxyFe[PF][1-MeIm],³⁵ since no comparable oxy cobalt porphyrin complex has yet been characterized. The iron atom was replaced with cobalt in the starting structure; otherwise the atoms within 5 Å of the metal atom were identical to the model compound. The methyl group of 1-MeIm is not included in the EXAFS analysis, since its backscattering signature is quite small. The starting structure is systematically modified by AUTOFIT's geometry program (see Materials and Methods) to provide input structures for the FEFF calculations and to provide a simulation that adequately models the data.

As have been shown previously,^{31,47} the EXAFS of metal-porphyrin systems is dominated by contributions of the four pyrrole rings. These are varied as a single unit in the simulations to obtain the best match to the data. There are three major distances of interest: average cobalt-pyrrole nitrogen distance

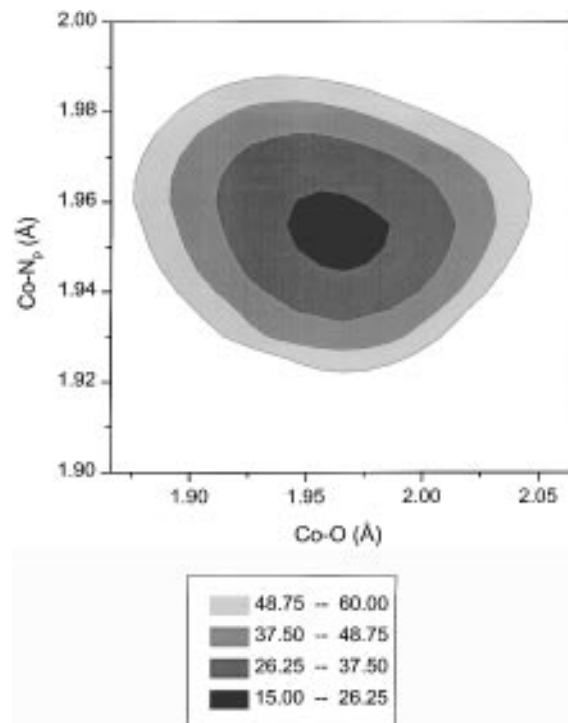


Figure 6. Global mapping of the cobalt-pyrrole nitrogen (Co-N_p) and cobalt-oxygen (Co-O) distances obtained from comparison of simulated EXAFS spectra to data for oxyCoTPP-1-MeIm in 100% toluene (Figure 5A, solid line). A total of 441 separate simulations were carried out, whereby the Co-N_p and Co-O distances were varied in increments of 0.005 and 0.01 Å, respectively, and the cobalt-axial imidazole nitrogen distance held constant at 2.07 Å. The darker shades in the contour plot represent better fits to the data.

(Co-N_p), cobalt-oxygen distance (Co-O), and cobalt-axial imidazole nitrogen distance (Co-N_{ax}), and two are varied at a time in three sets of pairs to find the best fit to the data.

As an example, in order to model the EXAFS data for oxyCoTPP-1-MeIm in 100% toluene, a grid of 441 separate FEFF simulations was carried out whereby the average Co-N_p versus Co-O distances were first varied, with the Co-N_{ax} distance fixed at the model compound³⁵ value of 2.07 Å. The results of the simulations are represented on a 3-D contour plot (Figure 6), where the *x*- and *y*-axes are the two metal-axial ligand distances in the simulation and the shading represents the ΣR² values (eq 3), with the darker shades corresponding to smaller ΣR² values or better fits. Next, a grid of simulations varying average Co-N_p versus Co-N_{ax} distances were carried out (not shown), with Co-O distance fixed at the 1.96 Å value obtained from the first set of simulations. These two sets of

(47) Binstead, N.; Strange, R. W.; Hasnain, S. S. *Biochemistry* **1992**, *31*, 12117.

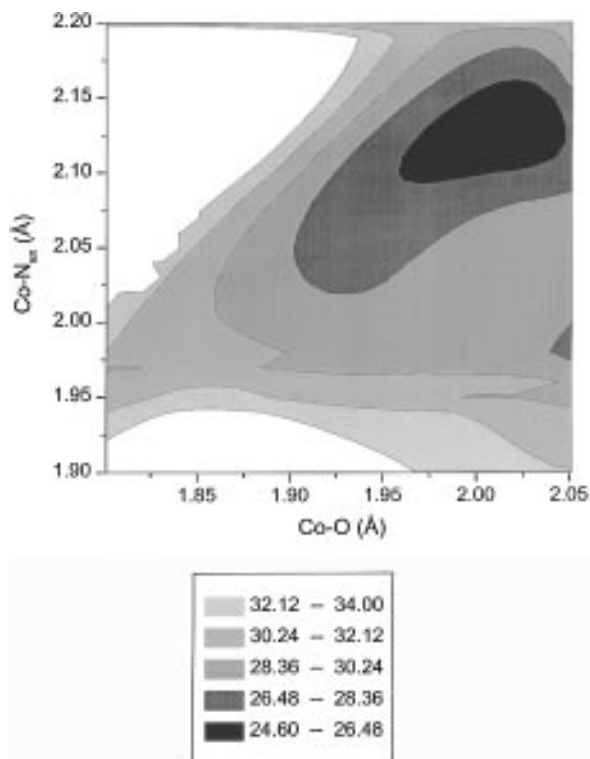


Figure 7. Global mapping of the cobalt-axial imidazole nitrogen (Co-N_{ax}) and cobalt-oxygen (Co-O) distances obtained from comparison of simulated EXAFS spectra to data for oxyCoTPP-1-MeIm in 100% toluene (Figure 5A, solid line). A total of 806 separate simulations were carried out, whereby the Co-N_{ax} and Co-O distances were varied in increments of 0.01 Å, and the cobalt-porphyrin nitrogen (Co-N_{p}) distance held constant at 1.96 Å. The darker shades in the contour plot represent better fits to the data. The sum of residuals represented by the white regions are larger than the highest range on the scale.

Table 3. EXAFS Bond Length Parameters of $\text{Oxy}(o\text{-R})_1\text{TPP-OxyCo-1-MeIm}$ Complexes

R	Co-N_{ax} (Å)	Co-O (Å)	Co-N_{p} (Å)
H (in 100% toluene)	2.12 ± 0.04	1.98 ± 0.03	1.96 ± 0.01
H (in 50% toluene, 50% CH_2Cl_2)	1.96 ± 0.03	1.97 ± 0.03	1.955 ± 0.015
$\text{NHCONHC}_6\text{H}_5$ (in 100% toluene)	1.94 ± 0.03	1.96 ± 0.01	1.94 ± 0.01

simulations gave identical values (1.96 \AA) for the average Co-N_{p} distance. This average Co-N_{p} distance was then fixed, while a grid of 806 separate FEFF simulations varying the Co-O and Co-N_{ax} distances were carried out and compared to EXAFS raw data. Here, the Co-O distance was varied from 1.80 to 2.05 Å in 0.01 Å steps, while the Co-N_{ax} distance was varied from 1.90 to 2.20 Å in 0.01 Å steps. The results of the simulations are similarly represented on a contour plot (Figure 7), where a clear minimum is seen at a Co-N_{ax} distance of $2.12 \pm 0.04 \text{ \AA}$ and a Co-O distance of $1.98 \pm 0.03 \text{ \AA}$, with an average Co-N_{p} distance of $1.96 \pm 0.01 \text{ \AA}$. The quality of the simulation using these metal-ligand bond distances can be seen in Figure 8, where it is compared to the background-subtracted EXAFS data.

Metal-ligand bond lengths are likewise obtained for oxyCoTPP-1-MeIm in 50% toluene/50% dichloromethane and for oxyCo[*o*-NHCONHC₆H₅]₁TPP-1-MeIm in toluene. The results are summarized in Table 3. The average Co-N_{p} and Co-O distances for the three complexes are not changed within the error, while the Co-N_{ax} distance was considerably shorter in oxyCoTPP-1-MeIm in 50% toluene/50% dichloromethane ($1.96 \pm 0.03 \text{ \AA}$) and in oxyCo[*o*-NHCONHC₆H₅]₁TPP-1-MeIm (1.94

$\pm 0.03 \text{ \AA}$) in toluene than in oxyCoTPP-1-MeIm in toluene ($2.12 \pm 0.04 \text{ \AA}$) (Table 3).

Discussion

Oxygen Affinity and Electronic Configuration of the Metal-Dioxygen Bond. Extensive functional studies of site mutants⁴⁸ and model compounds⁴⁹ of oxygen-carrying hemoproteins have demonstrated the role of the polarity of the distal heme pocket (the protein moiety surrounding the bound dioxygen) in governing oxygen affinity. For example, Traylor et al.^{50,51} found that the P_{50} of oxygen binding to chelated ferrous mesoporphyrin⁵² decreases from 4.9 to 2.8 Torr when the solvent is changed from 100% toluene to the more polar 90% toluene/10% dichloromethane (v/v) mixture.⁵³ Similar solvent effects on oxygen affinity of ferrous porphyrins have been reported by a number of laboratories and reviewed by Momenteau and Reed.⁴⁹ Alternatively, ferrous "picket fence" (PF) porphyrin [*meso*-tetrakis($\alpha,\alpha,\alpha,\alpha$ -*o*-pivalamidophenyl)porphyrin]^{14,54} (on which the [*o*-NHCO(CH₃)₃]₁TPP used in this study [Figure 1A] is based) and its derivatives exhibit increasing oxygen affinity with increased electron-withdrawing ability of the "pickets".⁴⁹ The "pickets" are believed to shield the bound dioxygen from the aprotic solvent and create a polar pocket so that an amide proton on the pickets can interact with the bound dioxygen as shown in Figure 1B, either through hydrogen bonding^{55,56} or electrostatically,^{56,57} depending on the nature of the picket. For example, when one of the four pivalamido pickets is replaced by a phenylurea group (on which the [*o*-NHCONHC₆H₅]₁TPP used in this study [Figure 1A] is based), oxygen affinity was found to increase 9-fold.¹⁶ These studies have thus convincingly demonstrated the role of a polar pocket surrounding the bound dioxygen in increasing oxygen affinity of ferrous porphyrins, even in the absence of a strong hydrogen bond to the bound dioxygen.^{56,57} These results have subsequently been reaffirmed by studies using myoglobin mutants which show that oxygen affinity increases in the presence of amino acids with polar side chains that are not necessarily hydrogen bond donor to the bound dioxygen.^{48,58,59}

Similar solvent^{60,61} and polar (refs 62, 63, and references therein) effects on oxygen affinity have been reported for

(48) Springer, B. A.; Sligar, S. G.; Olson, J. S.; Phillips, G. N., Jr. *Chem. Rev.* **1994**, *94*, 699.

(49) Momenteau, M.; Reed, C. A. *Chem. Rev.* **1994**, *94*, 659.

(50) Traylor T. G.; Chang, C. K.; Geibel, J.; Berzinis, A.; Mincey, T.; Cannon, J. J. *Am. Chem. Soc.* **1979**, *101*, 6716.

(51) Traylor, T. G.; Koga, N.; Deardurff, L. A.; Swepston, P. N.; Ibers, J. A. *J. Am. Chem. Soc.* **1984**, *106*, 5132.

(52) A ferrous mesoporphyrin in which an alkyl chain of appropriate length covalently connects a methylene carbon of a porphyrin pyrrole and a nitrogenous axial base of the ferrous ion.

(53) The dielectric constants for toluene and dichloromethane at room temperature is respectively 2.379 D at 25 °C and 9.08 D at 20 °C. (*Handbook of Chemistry and Physics*; CRC Press: Boca Raton, FL.)

(54) Collman, J. P.; Gague, R. R.; Reed, C. A.; Robinson, W. T.; Rodley, G. A. *Proc. Natl. Acad. Sci. U.S.A.* **1974**, *71*, 1326.

(55) Mispelter, J.; Momenteau, M.; Lavalette, D.; Lhoste, J.-M. *J. Am. Chem. Soc.* **1983**, *105*, 5165.

(56) Gerotheranassis, I. P.; Momenteau, M.; Loock, B. *J. Am. Chem. Soc.* **1989**, *111*, 7006.

(57) Jameson, G. B.; Drago, R. S. *J. Am. Chem. Soc.* **1985**, *107*, 3017.

(58) Rohlfs, R. J.; Mathews, A. J.; Theodore, T. E.; Olson, J. S.; Springer, B. A.; Egeberg, K. D.; Sligar, S. G. *J. Biol. Chem.* **1990**, *265*, 3168.

(59) Carver, T. E.; Rohlfs, R. J.; Olson, J. S.; Gibson, Q. H.; Blackmore, R. S.; Springer, B. A.; Sligar, S. G. *J. Biol. Chem.* **1990**, *265*, 20007.

(60) Yamamoto, H.; Takayani, T.; Kwan, T.; Yonetani, T. *Bioinorg. Chem.* **1977**, *7*, 189.

(61) Drago, R. S.; Cannady, P. J.; Leslie, K. A. *J. Am. Chem. Soc.* **1980**, *102*, 6014.

(62) Walker, F. A.; Balke, V. L.; West, J. T. In *Frontiers in Bioinorganic Chemistry*; Xavier, A. V., Ed.; VCH: Germany, 1986; pp 183-193.

(63) Collman, J. P.; Zhang, X.; Wong, K.; Brauman, J. I. *J. Am. Chem. Soc.* **1994**, *116*, 6245.

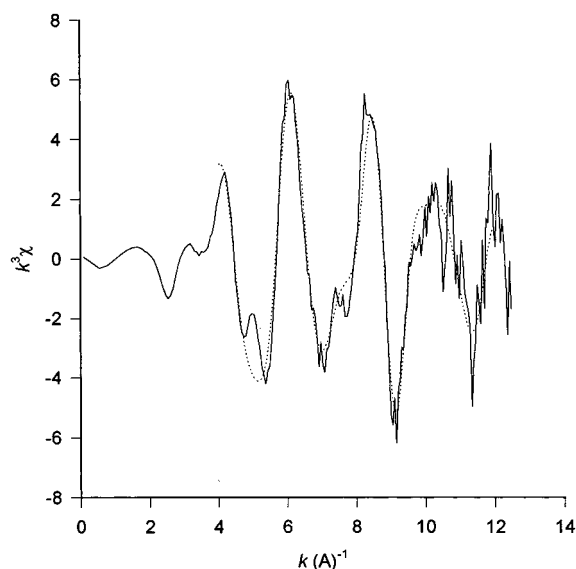


Figure 8. EXAFS data of oxyCoTPP-1-MeIm in 100% toluene (solid line) compared to simulation of data using FEFF 6.01 (dashed line), generated with an average Co–N_p distance of 1.96 Å, Co–N_{ax} distance of 2.12 Å and a Co–O distance of 1.98 Å as determined by the global mapping procedure outlined in the text (also see Figures 6 and 7). This simulation provides the best fit to the data from $k = 4\text{--}12 \text{ \AA}^{-1}$.

cobaltous porphyrins (for review, see Jones et al.⁶⁴). For example, Yamamoto et al.⁶⁰ found that for the pyridine complex of cobalt protoporphyrin IX dimethyl ester, the ΔG of O₂ binding at 25 °C is 1.5 kcal/mol more negative in *N,N*-dimethylformamide than in toluene. For the oxyCo[*o*-R]₁TPP-1-MeIm complexes used in this study (Figures 1 and 4), Walker et al.⁶² found that at –19 °C and in toluene, the O₂-association constants for R = –H, –NHCOC(CH₃)₃, and –NHCOC(CH₃)₃ are, respectively, 140, 210, and 1000 M^{–1}.

Cobalt-substituted hemoproteins also exhibit trends in oxygen affinity that parallel their iron counterparts (refs 5, 65 and references therein), suggesting similar structural factors govern the oxygen affinity of both the iron and the cobalt proteins. In contrast to the iron case, where a molecular orbital model⁶⁶ presents the binding of molecular oxygen to the ferrous heme iron as an oxidation process such that the σ -bonding orbital is given as $sp^2(N) + d_z^2(Fe^{3+}) + sp^2(O_2^{\bullet-})$, a molecular model for the cobalt–dioxygen unit⁶ suggested that the binding of molecular oxygen to the cobaltous ion needs not be represented as oxidation of the metal with the formation of a Co³⁺–O₂^{•–} bond. On the other hand, it is believed that increase in oxygen affinity for cobalt-substituted hemoproteins and models can be attributed to an increase in the oxygen character in the σ -bonding orbital $sp^2(N) + d_z^2(Co^{2+}) + \pi^*(O_2)$, i.e., an increase in the ionicity of the cobalt–dioxygen bond,³ and a shift toward the $sp^2(N) + d_z^2(Co^{3+}) + sp^2(O_2^{\bullet-})$ structure. This explains the parallel trends in oxygen affinity for native ferrous and cobalt-substituted hemoproteins (since structural factors that increase the ionicity of a cobalt–dioxygen bond should also stabilize a ferric superoxide structure).

ESEEM spectra of oxyCo hemoproteins and model compounds are useful probes for the ionicity of the cobalt–dioxygen bond. The magnitude of the ESEEM-revealed nuclear hyperfine and nuclear quadrupole couplings to an axial nitrogen reflect

the degree of oxygen character or ionicity of the cobalt–dioxygen bond.³ Reductions in ¹⁴N couplings have been consistently observed in protein and model complexes where the ionicity of the cobalt–dioxygen bond is expected to increase. This phenomenon was demonstrated in ESEEM studies of the natural and engineered mutants of oxyCo myoglobin, where the ionicity of the cobalt–dioxygen bond was altered as a result of substitution of the distal histidine, a hydrogen bond donor to the bound dioxygen, with non-hydrogen bond–donating amino acids of varying side-chain polarity. The presence of a hydrogen bond donor or a polar amino acid side chain in the vicinity of the bound dioxygen increases the ionicity of the cobalt–dioxygen bond and reduces axial ¹⁴N electron–nuclear couplings.^{3–5} In the present study, in systems where the ionicity of the cobalt–dioxygen is increased as a result of the increased polarity of the solvent (Figure 3) or in the presence of a more acidic proton nearby that can interact with the bound dioxygen^{14–16,62,67} (Figure 4), reductions in ¹⁴N electron–nuclear couplings again occur (Table 2).

¹⁴N Electron–Nuclear Coupling and Cobalt–Ligand Bond Length. ESEEM studies of oxyCo hemoproteins and models thus provide a direct demonstration that a more ionic cobalt–dioxygen bond is indeed associated with increase in oxygen affinity. Increase in ionicity is expected to result in a shorter cobalt–dioxygen bond while increased lone-pair electron donation from the axial nitrogen to the more positively charged cobalt will shorten the cobalt–axial nitrogen bond.¹⁰ The present study uses EXAFS spectroscopy to compare cobalt–ligand bond lengths of oxyCoTPP-1-MeIm in 100% toluene and in 50% toluene/50% dichloromethane as well as oxyCoTPP-1-MeIm with oxyCo[*o*-NHCONHC₆H₅]₁TPP-1-MeIm in toluene. Both electron–nuclear hyperfine and nuclear quadrupole coupling to the cobalt-bound 1-MeIm ¹⁴N decrease when the solvent polarity is increased or when an electron-withdrawing group is placed in the vicinity of the bound dioxygen of oxyCoTPP-1-MeIm (Table 2). EXAFS shows that the cobalt–axial nitrogen bond is shortened by $\sim 0.17 \text{ \AA}$, while the other bond lengths are relatively unaffected as the bound dioxygen is subjected to a more polar environment (Table 3).

The present EXAFS studies provide the first metal–ligand measurements for oxyCo porphyrin complexes with nitrogen base. The average cobalt–oxygen bond length of 1.96 Å (Table 3) found by EXAFS is typical of that found for oxyCo Schiff base complexes⁶⁴ studied by crystallography. Based on comparison with oxyCo Schiff base complexes and ferrous porphyrins, Jameson and Drago⁵⁷ have also estimated a cobalt–oxygen bond length of 1.95 Å for the 2-methylimidazole complex of oxyCo picket fence porphyrin.⁵⁴

For oxyCoTPP-1-MeIm in toluene, the cobalt–1-MeIm bond length of 2.12 Å is shorter (but within the error) than that for its deoxy counterpart in benzene,⁶⁷ 2.16 Å. For ferrous porphyrin with an unhindered axial imidazole ligand such as 1-MeIm, a shortening of the iron–axial nitrogen bond upon the binding of oxygen has also been found.^{35,68} On the other hand, the cobalt–porphyrin nitrogen bond length is similar for oxyCoTPP-1-MeIm in toluene (1.96 Å, Table 3) and its deoxy form in benzene (1.98 Å),⁶⁷ whereas for analogous ferrous systems,^{35,68} the iron–porphyrin nitrogen bond lengths are 1.98 and 2.07 Å in the oxy and deoxy compounds, respectively. This may be the result of a smaller metal out-of-plane displacement in the case of deoxyCoTPP-1-MeIm (0.14 Å)⁶⁷ as compared to that of 0.3 Å for the deoxy ferrous complex.⁶⁶

EXAFS measurements found shorter axial cobalt–nitrogen bonds for complexes exhibiting smaller nuclear quadrupole

(64) Jones, R. D.; Summerville, D. A.; Basolo, F. *Chem. Rev.* **1979**, *79*, 139.

(65) Ikeda-Saito, M.; Lutz, R. S.; Shelley, D. A.; McKelvey, E. J.; Materra, R.; Hori, H. *J. Biol. Chem.* **1991**, *266*, 23641.

(66) Reed, C. A.; Cheung, S. K. *Proc. Natl. Acad. Sci. U.S.A.* **1977**, *74*, 1780.

(67) Scheidt, W. R. *J. Am. Chem. Soc.* **1974**, *96*, 90.

coupling. A nuclear quadrupole resonance spectroscopy study of metal-imidazole complexes has used a Townes-Dailey⁶⁹ analysis to demonstrate that imino nitrogen is governed by the population of its p_σ orbitals.⁹ This idea is further investigated in the present study. The hypothesis is that if the imino nitrogen nuclear quadrupole is indeed governed by the p_σ population, then a decrease in nuclear quadrupole coupling signifies a decrease in the p_σ population, as a result of increased lone-pair electron donation to cobalt through an increase in the overlap of the nitrogen sp^2 hybrid and the cobalt d_z^2 orbital, and EXAFS should find a shorter cobalt-axial nitrogen distance. On the other hand, if the imino nitrogen nuclear quadrupole coupling is governed by its p_π population, then a decrease in nuclear quadrupole coupling indicates an decrease in p_π population, and by inductive effects,^{8,9} the p_σ population increases. This has to occur through decreased lone-pair electron donation to cobalt through decreased overlap of the nitrogen sp^2 hybrid and the cobalt d_z^2 orbital. In that case, EXAFS should find a longer cobalt-axial nitrogen distance with decrease in nuclear quadrupole coupling. The present EXAFS study finds shorter axial cobalt-nitrogen bonds for complexes exhibiting smaller nuclear quadrupole coupling, and provides further support for the idea that the imino nitrogen nuclear quadrupole coupling is indeed governed by the nitrogen p_σ population. Besides providing a molecular structural explanation for the change in nuclear quadrupole coupling, the current EXAFS results also demonstrate how molecular structures are related to functional properties. Shorter cobalt-axial nitrogen bonds are found for complexes with higher oxygen affinity. Shorter cobalt-axial nitrogen bonds, as discussed above, result from increased lone-pair donation from nitrogen to cobalt. This occurs with increased positive charge density on the metal or a more ionic/polar metal-oxygen bond that has also been shown to give rise to higher oxygen affinity.

In an ESEEM study of $(\alpha\text{Co}-\text{O}_2)_2(\beta\text{Fe}-\text{O}_2)_2$ and $(\alpha\text{Fe}-\text{O}_2)_2(\beta\text{Co}-\text{O}_2)_2$ hybrid hemoglobins, smaller nuclear hyperfine and nuclear quadrupole coupling were found for the oxyCo α subunits than for the oxyCo β subunits.¹⁰ It was suggested that the smaller nuclear hyperfine coupling found for the oxyCo α subunits signifies a more ionic and therefore shorter cobalt-oxygen bond, whereas the smaller nuclear quadrupole coupling indicates increase overlap of the sp^2 hybrid of the axial nitrogen with the cobalt d_z^2 orbital and thus a shorter cobalt-nitrogen bond. These results were considered to be consistent with a crystal structure of $(\alpha\text{Fe}-\text{O}_2)_2(\beta\text{Fe}-\text{O}_2)_2$,⁷⁰ which shows shorter Fe-O and Fe-N bonds for the oxyFe α subunits; they are also consistent with the higher oxygen affinity found for the oxyCo α than for the oxyCo β subunits.⁷¹ Similarly, longer Fe-O and Fe-N bonds have been found for the oxy α subunits of $(\alpha\text{O}_2\beta)_2$ Hb (T state, lower O_2 affinity) and the oxy α subunits of $(\alpha\text{O}_2\beta\text{O}_2)_2$ Hb (R state, higher O_2 affinity).^{72,73} Furthermore, the crystal structures of the 1-MeIm and 2-MeIm complexes of oxyFe[PF] also show that both the iron-oxygen and iron-axial

nitrogen bonds are shorter in the 1-MeIm complex which also has higher oxygen affinity.^{35,74}

This study finds that reduction of electron-nuclear hyperfine coupling occurs in oxyCoTPP model complexes with higher oxygen affinity that is accompanied by significant shortening of the cobalt-axial nitrogen (by an average of 0.17 ± 0.06 Å). The cobalt-oxygen bond, on the other hand, remains essentially unchanged. Hyperfine coupling parameters for the axial nitrogen obtained from simulation of ESEEM spectra indicate that this coupling is largely isotropic ($F [=g_e g_N \beta_e \beta_N / r^3] / A_{\text{iso}} < 10\%$, see Table 2). This supports the hypothesis that hyperfine coupling is governed by the electronic structure of the $sp^2(\text{N}) + d_z^2(\text{Co}^{2+}) + \pi^*(\text{O}_2)$ σ -bonding orbital⁶ and that for the compounds studied, reduction in axial nitrogen hyperfine coupling is a result of decreased cobalt character in this orbital,⁷ as reflected by the decrease in cobalt 3d orbital spin density (Table 1), or increased ionicity of the cobalt-oxygen bond. It is possible the differences in ionicity of the cobalt-oxygen bond among the complexes studied exhibit distinct changes in hyperfine coupling to the trans ligand but not in cobalt-oxygen bond length changes that can be revealed by EXAFS spectroscopy. It should be noted that given the error estimated for the measurement of the cobalt-oxygen bond length (Table 3), this distance for the complexes examined could differ by as much as 0.07 Å.

On the other hand, further studies are required to determine whether the concurrent shortening of both axial bonds applies only to oxy ferrous hemoproteins but not oxyCo hemoproteins, or whether this phenomenon is observed only in the more restricted Fe and Co protein environment and not in model compounds. It is possible that shortening of the cobalt-dioxygen is less favorable than for the iron-dioxygen bond, since the fully occupied $d\pi$ orbitals of cobalt would make ligand \rightarrow metal π bonding less likely in oxyCo than in oxyFe systems.

In summary, this study shows that for systems exhibiting higher oxygen affinity as a result of increased solvent polarity or of polar interactions, the cobalt-oxygen bond shifts toward a more ionic structure that is manifested in reduction of electron-nuclear coupling to the axial nitrogen ligand and a shortening of the cobalt-nitrogen bond. This correlation of electronic structure of cobalt-dioxygen bond of hemoprotein model complexes with electron-ligand nuclear coupling parameters and cobalt-axial nitrogen bond length change unequivocally exemplifies the intimate interrelationship among the electronic and molecular structures and oxygen affinity of model heme systems.

Acknowledgment. This work was supported by N.I.H. Grants GM40168 (J.P.), RR.02538 (J.P.), HL45892 (M.R.C.), and RR01633 (M.R.C.). Research carried out in part at the National Synchrotron Light Source, Brookhaven National Laboratory, which is supported by the U.S. Department of Energy, Division of Materials Sciences and Division of Chemical Sciences. H.C.L. is grateful to Professor F. Ann Walker (University of Arizona) and members of her laboratory, in particular Dr. Simone E. Jacobson, for sharing their expertise in porphyrin synthesis.

JA9717166

(68) Momenteau, M.; Scheidt, W. R.; Eigenbrot, C. W.; Reed, C. A. *J. Am. Chem. Soc.* **1988**, *110*, 1207.

(69) Townes, C. H.; Dailey, B. P. *J. Phys. Chem.* **1949**, *17*, 782.

(70) Shanaan, B. *J. Mol. Biol.* **1983**, *171*, 31.

(71) Imai, K.; Ikeda-Saito, M.; Yamamoto, H.; Yonetani, T. *J. Biol. Chem.* **1980**, *138*, 635.

(72) Brzozowski, A.; Derewende, Z.; Dodson, E.; Dodson, G.; Grabowski, M.; Liddington, R.; Skarżyński, T.; Valley, D. *Nature* **1984**, *307*, 74.

(73) Liddington, R.; Derewende, Z.; Dodson, G.; Harris, D. *Nature* **1988**, *331*, 725.

(74) Jameson, G. B.; Molinaro, F. S.; Ibers, J. A.; Collman, J. P.; Brauman, J. I.; Rose, E.; Suslick, K. S. *J. Am. Chem. Soc.* **1978**, *100*, 6769.

(75) Goodman, B. A.; Raynor, J. B. *Adv. Inorg. Chem. Radiochem.* **1970**, *13*, 135.